A New Configuration of Dual Stator Induction Generator Employing Series and Shunt Capacitors

Saptarshi Basak, *Student Member, IEEE*, Chandan Chakraborty, *Fellow, IEEE* and Bikash C. Pal, *Fellow, IEEE*

***Abstract*—Doubly-fed induction generators are suitable for systems having limited speed range as the overall control can be carried out by fractionally-rated converters. However, brushes and slip-rings used in these generators reduce system reliability and demand greater maintenance. Dual stator winding induction generator(DSWIG), being brushless, removes this limitation. Two distributed windings are embedded in the stator and the rotor is squirrel-cage. One of the windings is interfaced to an uncontrolled rectifier and the other to a fractionally rated PWM converter. Uncontrolled rectifier degrades the power quality within the generation system. At the same time, reactive power demand in induction generators increases with loading. This work deals with design and control of a standalone dc system based on DSWIG where a combination of passive tuned filter and series capacitor is utilised to address the voltage regulation and power quality issue. Simulation results using MATLAB/Simulink and experimental results (obtained from a laboratory prototype) have been presented, compared and discussed to demonstrate the effectiveness of the proposed alternative.**

***Keywords*—Brushless Generation Systems, Dual Stator Winding Induction Generator, Micro-Grid, Renewable Energy Extraction.**

List of Symbols

ω_e	Speed of rotating reference frame
ψ_{dr},ψ_{qr}	Rotor flux in rotating reference frame
ψ_{ds},ψ_{qs}	Controlled winding flux in rotating reference frame
ψ_{du},ψ_{qu}	Uncontrolled winding flux in rotating reference frame
I_{CW},I_{UW}	RMS values of controlled and uncontrolled winding currents
i_{CW},i_{UW}	Instantaneous values of controlled and uncontrolled winding currents in time-domain
i_{dcs},i_{dcu}	DC link currents of the converter connected to controlled winding and uncontrolled winding respectively
i_{dr},i_{qr}	Rotor currents in rotating reference frame
i_{ds},i_{qs}	Controlled winding currents in rotating reference frame
i_{du},i_{qu}	Uncontrolled winding currents in rotating reference frame
L_m	Mutual inductance between controlled/uncontrolled winding and Rotor
L_s, L_u, L_r	Self inductance of controlled, uncontrolled winding, and rotor respectively
L_{ls}, L_{lu}, L_{lr}	Leakage inductance of controlled, uncontrolled winding, and rotor respectively
L_{us}	Mutual Inductance between controlled and uncontrolled winding
m_{ds},m_{qs}	Modulation index reference for controlled-winding side converter in d-q reference frame
v_{dr},v_{qr}	Rotor voltages in rotating reference frame
v_{ds},v_{qs}	Controlled winding voltages in rotating reference frame
v_{du},v_{qu}	Uncontrolled winding voltages in rotating reference frame
k	Power sharing ratio

S.Basak and C.Chakraborty are with Department of Electrical Engineering, Indian Institute of Technology Kharagpur.
B.C.Pal is with Department of Electrical and Electronic Engineering, Imperial College London, SW7 2BT,London.
Corresponding author e-mail: s.basak.1987@ieee.org.
Manuscript received April 28, 2017; revised August 23, 2017; accepted October 2, 2017.

I. Introduction

DOUBLY-FED induction machines (DFIMs) have been found suitable for motor drives or generation systems where the speed-range of operation is limited as the control of the overall system can be performed by a fractionally rated converter connected on the rotor side [1]–[3]. Wind-energy conversion system forms one of the best examples of such application [4]. However, brushes and slip-rings are prone to failure and require regular maintenance. As a result, various efforts pursued with the development of generation systems or motor drives where the system is brushless and facilitates control of the overall system through fractionally-rated converters [5]. One such solution is brushless doubly-fed induction machine (BDFIM) [6], [7]. BDFIM comprises of two stator windings wound for different pole configuration and a nested-loop rotor. One of the windings is directly interfaced to the ac-grid and the other one through a back-to-back converter configuration (similar to DFIMs). However, such machines necessitate use of a specially-constructed nested-loop rotor, which is a disadvantage. In comparison, self-excited induction generators are rugged and can be easily manufactured [8]. However, speed-range of such systems is narrow. In order to make such systems suitable for variable-speed generation applications, a full-scale converter has to be placed on the stator terminals [9]. Use of an additional stator winding can assist in reducing controlled-converter rating to a great-extent, especially for dc-mircogrid applications [10]. The performance of dual stator winding induction machine (with different pole configuration of stator windings) in motoring mode of operation have been reported in [11]. Torque-sharing functions for the two stator windings in order to prevent core saturation has been dealt with in [12]. Control algorithms for open-end winding split-phase induction machines have been discussed in [13]. This machine has the capability to replace high-power, medium-voltage synchronous machine drive. One such contribution has been described in [14]. Voltage-frequency control using dual stator winding induction generator (DSWIG) for standalone ac load was formulated in the pioneering work in [15]. Subsequently, DSWIG has found increased attention for applications like power supplies for electric vehicle [16], more-electric aircraft [17] as well as wind electrical systems [18], [19]. DSWIG consists of a rugged squirrel cage rotor and two windings on the stator, namely power and control winding. Since the two windings are wound for same number of poles, they can influence each other through the electromagnetic coupling. Power-winding delivers active power to load and control-winding regulates the output

voltage with the help of a controlled converter connected across it. Since the main purpose of control-winding is to regulate excitation, the controlled converter rating is much less compared to the overall rating of generation system. Performances of the system for balanced and unbalanced loading have been investigated in [20] and [21] respectively. If the application demands supplying to a standalone dc load, power-winding voltage is rectified using a diode bridge rectifier. Controller development for wide-speed range operation of DSWIG has been reported in [22] where the boost capability of control winding converter has been utilised to extend the speed range. Comparative study of different control strategies for standalone dc system has been performed in [23]. Standalone dc systems using DSWIG having two stator windings of different pole configuration has been discussed in [24]. However, such systems necessitate use of two separate PWM converters corresponding to two stator windings, which is a drawback from the perspective of controlled switch count. As reported in the literature, the system can work with a combination of uncontrolled and PWM rectifier (with two separate dc-links) and without the compensation of lower order harmonics. However, such a system will have more losses (due to increased THD of the winding currents) and the output power capability will degrade. For the same output power, the windings need to handle more current. Unlike that of DFIG based systems reported in [25]–[28], DSWIG comprises of three magnetically coupled windings. It becomes difficult to compensate for the harmonics by using the controlled winding side converter alone. Therefore, shunt passive filters are deployed at the terminals of the winding which is interfaced to the uncontrolled rectifier so as to mitigate the effect of harmonics at the source itself. It is also well known that induction generators demand reactive power with increase in load. This requirement has motivated the authors to provide compensation in series with the load. Adversely the system now requires more number of capacitors, which reduce reliability. However, modern film capacitors have low value of effective series resistance that makes them less dissipative and so increases life-span. Also, series capacitors possess the ability to bring about a reactive power change in the right direction. This enhances the stability to a great extent and the system offers self-regulation features. Voltage-collapse that is a frequent phenomenon for self-excited induction generators can be completely eliminated by a proper system-design employing series-capacitors. The main contributions presented in this paper are: (i) development of a different configuration of DSWIG which is self-regulatory in nature, (ii) design of passive elements in order to improve voltage regulation, and (iii) stability improvement aided through incorporation of series capacitance.

This paper consists of seven sections. Complete system description, mathematical model and design of passive elements are presented in Section-II. Section-III analyses and compares the stability of the system with and without series capacitor. Section-IV deals with the formulation of controller. MATLAB/Simulink based simulation results are presented in Section-V. A dSPACE 1103 based laboratory prototype has been fabricated and experimental results obtained using it is reported in Section-VI. Section-VII concludes the work.

II. Proposed Topology

A. System description

This subsection provides a detailed description of the system functionalities (corresponding to the topology in Fig. 1). The stator of DSWIG consists of two windings which are wound for the same number of poles so that they are magnetically coupled. The rotor is a squirrel cage type. Since the windings are magnetically coupled, the variables of one winding can directly influence the other. Thus, the converter connected to controlled winding (CW) will regulate the excitation within the machine, thereby controlling the induced voltage on the uncontrolled winding (UW) side. A three-phase diode bridge rectifier rectifies this voltage and establishes the dc-bus voltage v_{dc}. Therefore, through excitation control on the controlled winding, v_{dc} can be regulated. The two converters share a common dc-bus. This minimizes the number of electrolytic capacitors and creates a path for simultaneous active power flow through both the windings. This is made possible by connecting the UW in star and CW in delta, as a voltage gain of $\sqrt{3}$ from CW to UW is introduced. This is necessary as a buck-type operation takes place as seen from CW to UW side. Supporting derivation is included in Appendix B. For this particular generator, it is possible to use a parallel combination of uncontrolled and controlled rectifier as active power flow is unidirectional and the reactive power is supplied by a combination of shunt capacitors C_{sh}, series capacitance C_{se} and controlled winding side converter(CWSC). The presence of diode bridge rectifier (which shares major portion of the power, especially near to rated speed of operation) will have a detrimental effect on the generating system as the power quality and the power factor will degrade. Thus, a proper configuration of passive elements is necessary to deal with this issue. Tuned passive filters can assist in improving power quality as well as providing some amount of reactive power support at fundamental frequency. However, reactive power demand in induction generators increases with load, which degrade voltage regulation. Therefore, a combination of series and shunt capacitors have been chosen as an effective solution. Series capacitance can provide reactive power compensation in proportion to load current and thus assists in improving voltage regulation and increasing power output from the machine.

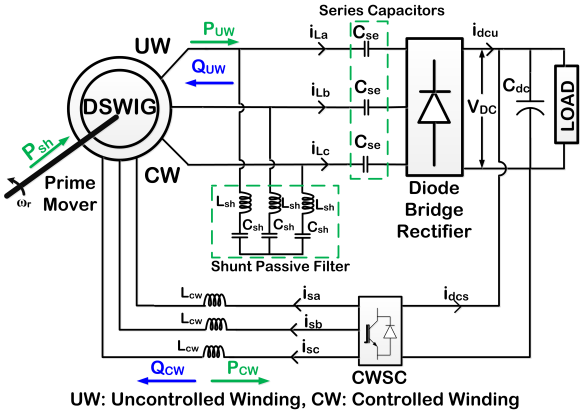

Fig. 1. Proposed configuration of a standalone dc generating system based on DSWIG (with tuned passive filters and series capacitance)

B. Mathematical Modelling

Simulation model of DSWIG has been developed in MATLAB/Simulink. The following equations given by (1)-(6) describes the model in arbitrary reference frame [15].

$$v_{du} = R_u i_{du} + \frac{d\psi_{du}}{dt} - \omega_e \psi_{qu} \tag{1}$$

$$v_{qu} = R_u i_{qu} + \frac{d\psi_{qu}}{dt} + \omega_e \psi_{du} \tag{2}$$

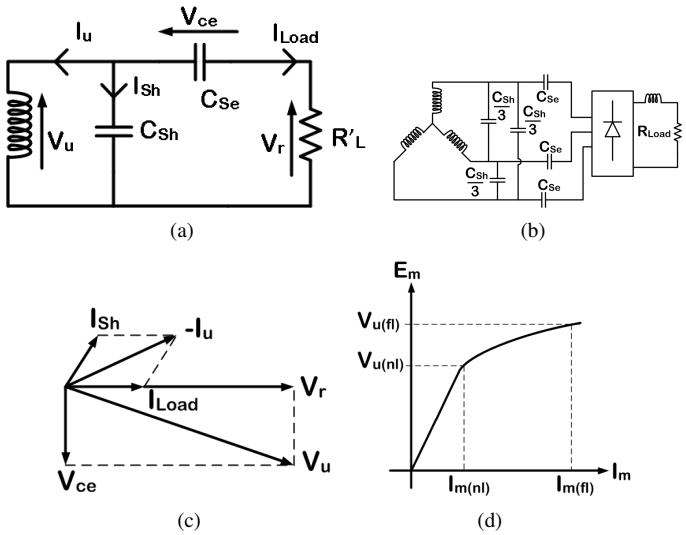

Fig. 2. (a) Schematic diagram demonstrating the uncontrolled winding side of the generating system (b) Single-phase equivalent circuit of the uncontrolled winding side network (c) Corresponding phasor diagram (d) Definition of $V_{t(nl)}$ and $V_{t(fl)}$ from a representative magnetization curve

.

$$v_{ds} = R_s i_{ds} + \frac{d\psi_{ds}}{dt} - \omega_e \psi_{qs} \tag{3}$$

$$v_{qs} = R_s i_{qs} + \frac{d\psi_{qs}}{dt} + \omega_e \psi_{ds} \tag{4}$$

$$v_{dr} = R_r i_{dr} + \frac{d\psi_{dr}}{dt} - (\omega_e - \omega_r)\psi_{qr} \tag{5}$$

$$v_{qr} = R_r i_{qr} + \frac{d\psi_{qr}}{dt} + (\omega_e - \omega_r)\psi_{dr} \tag{6}$$

Since the rotor is squirrel cage, $v_{dr} = v_{qr} = 0$. The inductance matrix is given by:

$$\begin{bmatrix} \psi_{du} \\ \psi_{qu} \\ \psi_{ds} \\ \psi_{qs} \\ \psi_{dr} \\ \psi_{qr} \end{bmatrix} = \begin{bmatrix} L_u & 0 & L_{us} & 0 & L_m & 0 \\ 0 & L_u & 0 & L_{us} & 0 & L_m \\ L_{us} & 0 & L_s & 0 & L_m & 0 \\ 0 & L_{us} & 0 & L_s & 0 & L_m \\ L_m & 0 & L_m & 0 & L_r & 0 \\ 0 & L_m & 0 & L_m & 0 & L_r \end{bmatrix} \begin{bmatrix} i_{du} \\ i_{qu} \\ i_{ds} \\ i_{qs} \\ i_{dr} \\ i_{qr} \end{bmatrix} \tag{7}$$

C. Design of shunt filter and series capacitance

*Design of shunt filter:*The purpose of the shunt passive filter is not only to improve power quality but also provide some required amount of reactive power support which will be useful for improving voltage regulation. The filter is designed to absorb significant and predominantly lower order harmonics and cater to the no-load reactive power demand. Therefore, the following per-phase reactive power balance equation has to be satisfied:

$$V_{t(nl)}\, I_{m(nl)} = \omega_{e(nl)}\, V_{t(nl)}^2\, C_{sh} \tag{8}$$

Here, $I_{m(nl)}$ refers to the magnetization current corresponding to the no-load terminal voltage. $I_{m(nl)}$ can be obtained from the magnetization characteristics (as shown in Fig. 2(d)). To optimally cancel out the predominant lower-order harmonics, the shunt filter has been tuned for m^{th} harmonic given by (9) [29].

$$m = \sqrt{\frac{49(25\alpha_5)^2 + 25(49\alpha_7)^2}{(49\alpha_7)^2 + (25\alpha_5)^2}} \tag{9}$$

where, $\alpha_5 = \frac{I_5}{I_1}$ and $\alpha_7 = \frac{I_7}{I_1}$. Here, I_1, I_5 and I_7 corresponds to the rms values of fundamental, fifth and seventh harmonic components of uncontrolled winding current in absence of tuned filter. Using typical values of α_5 and α_7 as 0.1995 and 0.1 respectively, the value of shunt filter inductor L_{sh} can be obtained from the relation in (10).

$$L_{sh} = \frac{1}{(m\,\omega_e)^2\, C_{sh}} \tag{10}$$

Using (8) and (10), the value of shunt capacitor and inductor turns out to be 34 μF and 10.65 mH.

Design of series capacitance: For the sake of simplicity, the schematic diagram in Fig. 2(a) shows the uncontrolled winding side of the generating system. A simplified equivalent circuit is demonstrated in Fig. 2(b). Here, R'_L is the reflected resistance on the uncontrolled winding side of the diode rectifier, which is given by $R'_L = \frac{\pi^2}{18} R_{Load}$ [30]. The phasor diagram corresponding to the simplified equivalent circuit is shown in Fig. 2(c). Since the same load current flows through C_{se} and equivalent load resistance, the two voltages V_r and V_{ce} are orthogonal to each other. Therefore, the following expression can be written:

$$V_{ce} = I_{Load} X_{se} = \sqrt{V_u^2 - V_r^2} \tag{11}$$

Let, $V_{u(fl)}$ be the full-load uncontrolled winding terminal voltage and $V_{u(nl)}$ be the corresponding no-load value. Definition of these two quantities are illustrated using Fig. 2(d). Given a percentage allowable voltage drop across C_{se}, the value of C_{se} can be estimated by:

$$C_{se} = \frac{I_{Load}}{\omega_{e(fl)} \sqrt{V_{u(fl)}^2 - V_{u(nl)}^2}} \tag{12}$$

Here, $\omega_{e(fl)}$ corresponds to the generator terminal frequency at full-load, which can be estimated by the method described in [31]. From the magnetization curve of the machine, $V_{u(fl)}$ is taken as 120 V. The no-load voltage is obtained using the expression given by, $V_{u(nl)} = \frac{\pi}{3\sqrt{6}} v_{dc}$. The value of C_{se} computed using (12) is 221 μF.

III. Stability studies

This section discusses the stability improvement of the system with incorporation of series capacitance over the system with only passive tuned filter. It is important to estimate the variation of magnetizing inductance with load resistance and operating

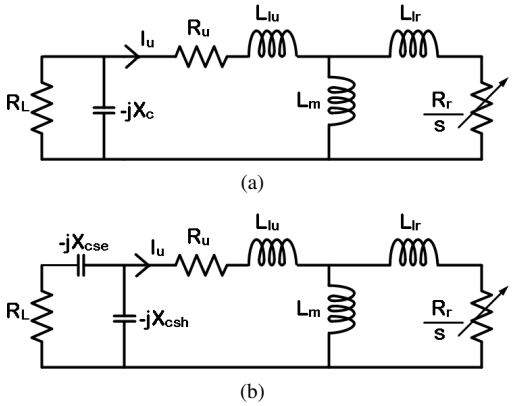

Fig. 3. Equivalent circuit of the uncontrolled winding side of DSWIG with (a) only shunt capacitance (b) series capacitance.

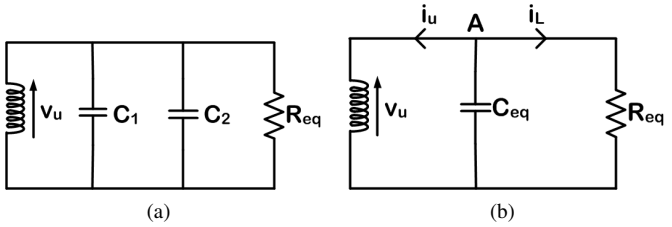

Fig. 4. (a) Equivalent shunt network corresponding to the circuit shown in Fig. 2(b), (b) Uncontrolled winding side network represented as a parallel combination of a resistance and capacitance.

frequency, which are the two important parameters while assessing the stability of induction generator systems. Fig. 3 displays the corresponding equivalent circuits. Applying loop equations, the circuit can be solved using $\Sigma I_u Z_u = 0$. Since $I_u \neq 0$, the circuit can be solved by equating the real and imaginary parts of ΣZ_u to 0. The two resulting simultaneous non-linear equations are solved to obtain the values of the L_m and ω_e for various load. For the system with only shunt compensation, $\Sigma Z_u = 0$ yields the expressions given by (13) and (14). Applying the same condition for the equivalent circuit in Fig. 3(b), relationships (15) and (16) are obtained.

$$\frac{1}{R'_L} + \frac{1}{\omega_e}\Big(1 + \frac{R_u}{R'_L} - \omega_e^2 L_{lu} C_{sh}\Big)\frac{R_r(\omega_e - \omega_r)}{R_r^2 + L_{lr}^2(\omega_e - \omega_r)^2} + \Big(\frac{L_{lr}(\omega_e - \omega_r)^2}{R_r^2 + (\omega_e - \omega_r)^2 L_{lr}^2} + \frac{1}{L_m}\Big)\Big(\frac{L_{lu}}{R'_L} + C_{sh}R_u\Big) = 0 \tag{13}$$

$$\omega_e^2 C_{sh} - \Big(1 + \frac{R_u}{R'_L} - \omega_e^2 C_{sh} L_{lu}\Big)\Big(\frac{L_{lr}(\omega_e - \omega_r)^2}{R_r^2 + (\omega_e - \omega_r)^2 L_{lr}^2} + \frac{1}{L_m}\Big) + \omega_e\Big(\frac{L_{lu}}{R'_L} + C_{sh}R_u\Big)\Big(\frac{R_r(\omega_e - \omega_r)}{R_r^2 + L_{lr}^2(\omega_e - \omega_r)^2}\Big) = 0 \tag{14}$$

$$R_u - \frac{C_{res}^2 R'_L}{C_{sh}}\frac{\frac{1}{C_{se}} - \frac{1}{C_{res}}}{1 + (\omega_e R'_L C_{res})^2} + \frac{(\omega_e - \omega_r)\omega_e L_m^2 R_r}{(R_r)^2 + (\omega_e - \omega_r)^2 L_r^2} = 0 \tag{15}$$

$$\omega_e L_{lu} - \frac{C_{res}}{\omega_e C_{sh} C_{se}}\Big[\frac{1 + (\omega_e R'_L)^2 C_{se} C_{res}}{1 + (\omega_e R'_L C_{res})^2}\Big] + \frac{\omega_e L_m [R_r^2 + (\omega_e - \omega_r)^2 L_{lr} L_r]}{(R_r)^2 + (\omega_e - \omega_r)^2 L_r^2} = 0 \tag{16}$$

Here, C_{res} is the effective capacitance given by $C_{res} = \frac{C_{se}C_{sh}}{C_{se}+C_{sh}}$.
At fundamental frequency, the passive tuned filter behaves as a capacitive circuit. Therefore, it is represented as a 'frequency-dependent' capacitive element C_1, as shown in Fig. 4(a). Similarly, the series combination of C_{se} and R'_L are transformed into a shunt equivalent circuit given by a load dependent capacitive element C_2 and a 'frequency-dependent' resistance R_{eq}. The parallel combination of C_1 and C_2 is represented as C_{eq} (referring to Fig. 4(b)). The mathematical expressions of C_1, C_2 and R_{eq} are given by:

$$C_1 = \frac{C_{sh}}{1 - \omega_e^2 L_{sh} C_{sh}},\ C_2 = \frac{C_{se}}{1 + (\omega_e C_{se} R'_L)^2},\ R_{eq} = \frac{1 + (\omega_e C_{se} R'_L)^2}{\omega_e^2 C_{se}^2 R'_L} \tag{17}$$

Using (10), the capacitance C_1 can be expressed as $C_1 = \frac{C_{sh}}{1 - \frac{1}{m^2}}$. So, C_1 is independent of frequency. For light load conditions, $(R'_L \omega_e C_{se})^2 \gg 1$. Using this approximation, following expressions are obtained:

$$C_2 \approx \frac{1}{(R'_L \omega_e)^2 C_{se}},\ R_{eq} \approx R'_L \tag{18}$$

Therefore, at light load conditions, $C_2 \propto \frac{1}{\omega_e^2}$ and R'_{eq} becomes independent of frequency, whereas at higher loads $R'_{eq} \propto \frac{1}{\omega_e^2}$ and C_2 is independent of frequency. For the configuration with only shunt filter, $C_{eq} = C_1$ and $R_{eq} = R'_L$, which are independent of frequency. The uncontrolled winding terminal voltage dynamics (obtained by applying KCL at node 'A') can be described by (referring to Fig. 4(b)):

$$C_{eq}\frac{dv_u}{dt} = -(i_u + i_L) \tag{19}$$

The machine model, given by (1)-(6), can be re-framed in terms of machine flux linkages as given by:

$$\dot{\psi_{du}} = -(a_{11}\psi_{du} + a_{12}\psi_{ds} + a_{13}\psi_{dr})R_u + \omega_e \psi_{qu} + v_{du} \tag{20.1}$$

$$\dot{\psi_{qu}} = -(a_{11}\psi_{qu} + a_{12}\psi_{qs} + a_{13}\psi_{qr})R_u - \omega_e \psi_{du} + v_{qu} \tag{20.2}$$

$$\dot{\psi_{ds}} = -(a_{21}\psi_{du} + a_{22}\psi_{ds} + a_{23}\psi_{dr})R_s + \omega_e \psi_{qs} + v_{ds} \tag{20.3}$$

$$\dot{\psi_{qs}} = -(a_{21}\psi_{qu} + a_{22}\psi_{qs} + a_{23}\psi_{qr})R_s - \omega_e \psi_{ds} + v_{qs} \tag{20.4}$$

$$\dot{\psi_{dr}} = -(a_{31}\psi_{du} + a_{32}\psi_{ds} + a_{33}\psi_{dr})R_r + (\omega_e - \omega_r)\psi_{qr} \tag{20.5}$$

$$\dot{\psi_{qr}} = -(a_{31}\psi_{du} + a_{32}\psi_{ds} + a_{33}\psi_{dr})R_r - (\omega_e - \omega_r)\psi_{dr} \tag{20.6}$$

The constants $a_{i,j}$ and Δ_L in (20) are given by:

$$a_{11} = \frac{L_s L_r - L_m^2}{\Delta_L},\ a_{12} = a_{21} = \frac{L_m^2 - L_{us} L_r}{\Delta_L},\ a_{13} = a_{31} = \frac{L_m(L_{us} - L_s)}{\Delta_L}, a_{22} = \frac{L_u L_r - L_m^2}{\Delta_L},\ a_{23} = a_{32} = \frac{-L_m(L_u - L_{us})}{\Delta_L}, a_{33} = \frac{L_u L_s - L_{us}^2}{\Delta_L}$$
$$\Delta_L = L_u(L_s L_r - L_m^2) - L_{us}(L_{us} L_r - L_m^2) + L_m^2(L_{us} - L_s) \tag{21}$$

Similarly with machine current expressed in terms of flux linkages, the behaviour of the terminal voltage across the uncontrolled winding in synchronously rotating reference frame is represented as:

$$\frac{dv_{du}}{dt} = -\frac{v_{du}}{\tau_{eq}} - \frac{a_{11}\psi_{du} + a_{12}\psi_{ds} + a_{13}\psi_{dr}}{C_{eq}} + \omega_e v_{qu}$$
$$\frac{dv_{qu}}{dt} = -\frac{v_{qu}}{\tau_{eq}} - \frac{a_{11}\psi_{qu} + a_{12}\psi_{qs} + a_{13}\psi_{qr}}{C_{eq}} - \omega_e v_{du} \tag{22}$$

where $\tau_{eq} = R_{eq}C_{eq}$. The machine model (given by (20)) and UW terminal voltage dynamics (given by (22)) are clubbed together to form the state space model in terms of $\dot{\underline{x}} = A\underline{x} + B\underline{u}$. Here, the states and inputs are defined as $\underline{x} = [\psi_{du}\ \psi_{qu}\ \psi_{ds}\ \psi_{qs}\ \psi_{dr}\ \psi_{qr}\ v_{du}\ v_{qu}]$ and $\underline{u} = [v_{ds}\ v_{qs}]$.
Corresponding to the each value of load resistance, the corresponding value of L_m and stator frequency is recorded (using the equivalent circuits shown in Fig. 3) and fed in to the stability analysis program. Eight eigenvalues will result from A-matrix,

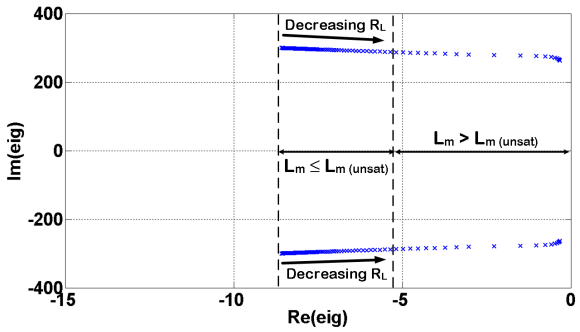

(a)

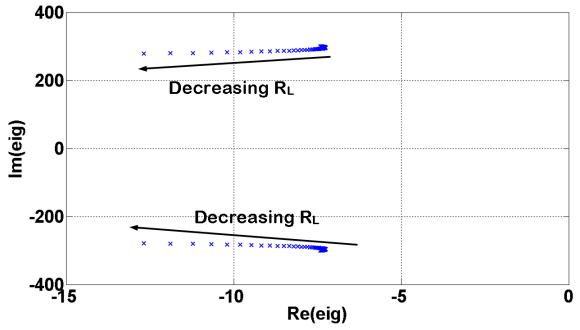

(b)

Fig. 5. Movement of pole locations with respect to variation in load resistance ($R_L = 20\Omega$ to $R_L = 200\Omega$) for the configurations with (a) shunt-filter only and (b) a combination of series capacitance of 221 μF and shunt passive filter. The values of L_{sh} and C_{sh} are provided in Appendix A

out of which two of them are found to be dominant. Fig. 5(a) shows the variation of these dominant pole locations with respect to load resistance for the configuration with shunt-filter only. It is interesting to note that the poles begin to move towards the right-half of s-plane with the reduction in load resistance. The values of L_m obtained using the equation $\Sigma I_u Z_u = 0$ exceeds the unsaturated value of L_m (i.e. $L_m > L_{m(unsat)}$), which is not a feasible solution. However, it is important to note the movement of poles with load resistance corresponding to the two different configurations. The behaviour of the system changes when series capacitors are introduced. The dominant poles move more into the left-half of s-plane with reduction in load resistance, as demonstrated in Fig. 5(b). Therefore, it can be inferred that deployment of series capacitance enhances the dynamic stability of the system.

IV. Description of Control Algorithm

Here, controlled-winding flux oriented control (CWFOC) has been adopted in order to regulate dc-link voltage to its desired value. In steady-state, the active and reactive power handled by the controlled winding is expressed as (with respect to the arrow directions in Fig. 1):

$$P_{CW} = -\frac{3}{2}(v_{qs}i_{qs} + v_{ds}i_{ds}) = -R_s(i_{ds}^2 + i_{qs}^2) - \frac{3}{2}\omega_e\psi_{ds}i_{qs}$$
$$Q_{CW} = \frac{3}{2}(v_{qs}i_{ds} - v_{ds}i_{qs}) = \frac{3}{2}\omega_e\psi_{ds}i_{ds} \quad (23)$$

From (23), it is evident that active power control through controlled-winding is possible through i_{qs} (if R_s is neglected) and that of reactive power through i_{ds}. In the proposed topology, reactive power contribution on the uncontrolled-winding side comes from two sources, (i) C_{sh}, which generates a fixed amount (ii) C_{se}, which generates reactive power in proportion to load current. The reactive power deficit or excess has to be adjusted by Q_{CW}. Thus, i_{ds} reference is generated from the v_{dc} PI controller such that the total reactive power demand (to keep v_{dc} regulated) within the generation system is met. The q-axis current (i.e. i_{qs}) consists of two components (as shown in Fig. 6): (i) i_{qsL}, which is proportional to the load and (ii) i_{qsE} which is proportional to the error between actual and reference value of dc-bus voltage. Power sharing ratio, k, takes care how much active power CWSC will carry. Detailed mathematical derivation of i_{qsL} generation technique is available in [29]. The vector rotater is generated using the reference voltages ($v_{s\alpha}$,$v_{s\beta}$) and controlled-winding side currents $i_{s\alpha}$,$i_{s\beta}$ using the following relationships, where $\vec{v_s} = v_{s\alpha} + jv_{s\beta}$ and $\vec{i_s} = i_{s\alpha} + ji_{s\beta}$:

$$\vec{\psi_s} = \int(\vec{v_s} - R_s\vec{i_s}) \quad (24.1)$$
$$\rho_e = arg(\vec{\psi_s}) \quad (24.2)$$

V. Simulation Results

Simulation studies are conducted in MATLAB/Simulink in order to explore the merits of the proposed topology. Dynamic performance of the controller along with harmonic reduction in phase currents are demonstrated through the simulation studies at a constant speed of 1500 r/min. The suitability of the system for variable speed operation has also been investigated. Table-I provides machine parameters used for simulation. All the parameters are referred to the controlled winding side.

A. Dynamic performance at constant speed

First, the system performance under step change in load is studied. Before $t = 3$ s, the system is running at no-load. A step-change in load of 0.5 kW occurs at $t = 3$ s as shown in Fig. 7(d). In order to restore the voltage to 220 V after an initial dip, i_{ds} increases from -1.1 to -0.1 A. Since i_{qs} reference is generated in proportion to load current, it changes to -2 A with negative sign indicating generating mode of operation. An additional load of 500 W is switched on at $t = 4$ s, which results in an increase of i_{ds} from -0.1 A to 0.6 A. It is interesting to note the effect of power-sharing ratio k on Δi_{ds} (i.e. the change in the value of i_{ds}) during the step change in load. When the power sharing ratio is changed to 0.2, the steady-state value of Δi_{ds} reduces to 0.35 A (as shown in Fig. 7(c)). With the decay in the value of k, more power is pumped through the uncontrolled-winding causing more current to flow through C_{se} making the system more self-regulatory. Thus, control effort reduces with the reduction in the value of k. Since $i_{qs} \propto k$, the value of i_{qs} becomes almost half for a particular value of load current when k reduces from 0.4 to 0.2, as noticeable from Fig. 7(b) and 7(c). The dc bus voltage and load current dynamics are of similar nature for $k = 0.2$ and hence, are not illustrated again.

B. Steady state waveforms

Fig. 8 shows the steady phase current waveforms for a load of 1 kW corresponding to a power sharing ratio (k) of 0.4. The passive tuned filters have been instrumental in improving the power quality to a great extent, as shown in Fig. 8(a) and 8(b). Fig. 8(c) reveals that the fifth and seventh harmonic component of current can be brought to less than 2% of the fundamental component of current. Similarly, the predominant lower order harmonics in uncontrolled winding current can be reduced to less than 3% of the fundamental current. The RMS value of

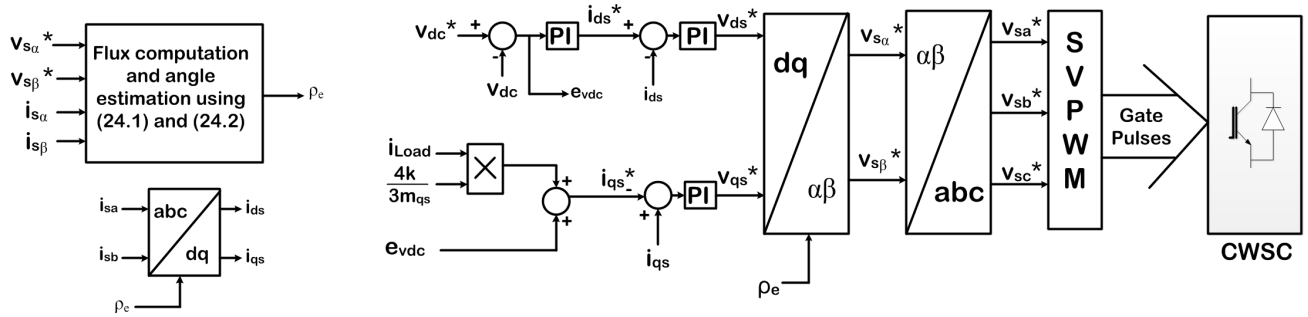

Fig. 6. Block diagram showing dc-bus voltage controller (with a provision to regulate power shared among each stator winding)

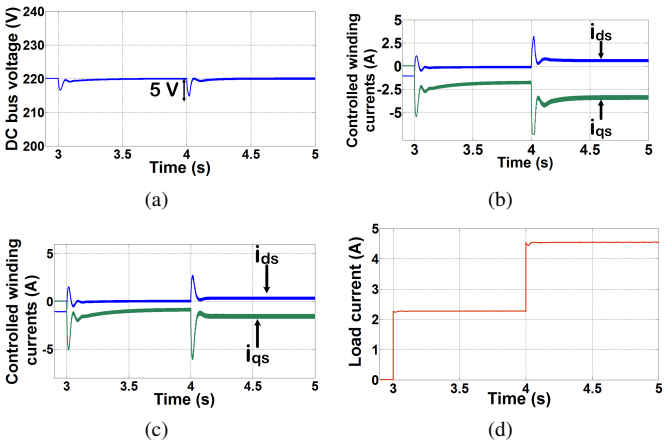

Fig. 7. (a) DC Bus voltage dynamics due to a step change in load for $k = 0.4$ (b) Response of the controlled winding currents when there is a step change in load for $k = 0.4$ (c) Response of i_{ds} and i_{qs} during step change in load for $k = 0.2$ (d) Discrete changes in load current

controlled winding current waveform is 2.01 A and that of uncontrolled winding current is 3.68 A. The THD of the i_{UW} is 3.02% while that of i_{CW} is 4.25%.

C. Performance for change in speed

Fig. 9 demonstrates the performance of the system when there is gradual decrease in prime mover speed. If wind electrical system is considered to be the target application, maximum available power from wind will reduce in cubic proportion to prime mover speed (i.e. $P_{out} \propto \omega_m^3$). Thus, the maximum available power at 0.6 p.u. speed is 0.216 p.u. with 1 p.u. speed

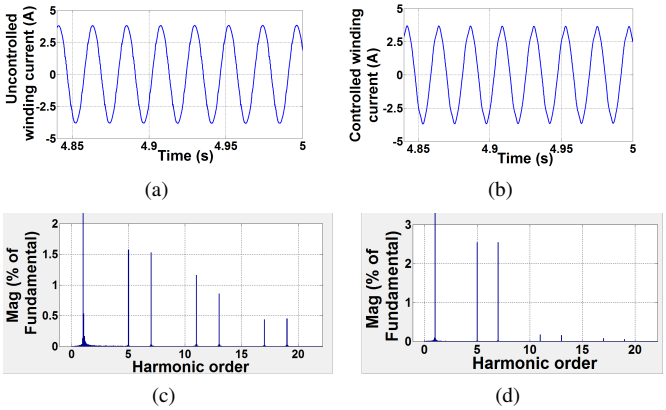

Fig. 8. Line current waveform for (a) uncontrolled and (b) controlled winding current at a load of 1 kW for $k = 0.4$. Line current spectra for (c) uncontrolled and (d) controlled winding current for same load and power sharing factor.

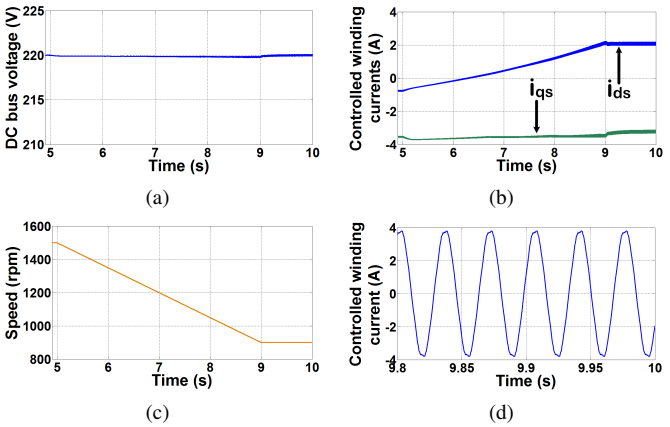

Fig. 9. (a) DC bus voltage dynamics during gradual change in speed (b) Response of controlled winding currents (in rotating reference frame) (c) Decay in speed (d) Steady-state waveform of controlled winding line current

corresponding to a speed of 1500 rpm. Fig. 9(c) shows the variation of prime mover speed from its rated value to 0.6 p.u. As shown in Fig. 9(a), dc bus voltage is held fairly constant by means of i_{ds} control, irrespective of this speed change. From Fig. 9(b), it can be seen that i_{ds} increases from -0.6 A to 2 A in order to regulate dc bus to 220 V. Since load on the system is constant, i_{qs} remains fairly constant at -3.5 A. Fig. 9(d) illustrates the steady-state phase current waveform at a prime mover speed of 900 r/min. The rms value of line current is 2.72 A and its THD is 2.28%.

VI. Experimental Results

A. Dynamic performance during loading

Performance of the system when subjected to a sudden rise in load has been experimentally validated and reported here. A dc machine coupled to DSWIG serves the purpose of a prime mover which drives the generation system at a speed of 1500 r/min. Experimental results are presented for two values of k i.e. $k = 0.4$ and $k = 0.2$. Initially, a load of 0.5 kW is present across the dc-bus and another 0.5 kW load is applied at $t = 1.5$ s. As result of this sharp change in load, v_{dc} undergoes an initial dip of 6 V and is restored to its original value of 220 V within 0.2 s (referring to Fig. 10(a)). The controlled-winding d-axis current increases from -0.5 A to 0, as shown in Fig. 10(c). The reduction in Δi_{ds} with reduction in k has been experimentally verified. When k becomes 0.4, the steady-state value of i_{ds} changes from -0.5 to 0.5 A (as depicted in Fig. 10(b)). This is due to increased current flow through series capacitors which provides better voltage regulation capability. Corresponding simulation results show that the steady-state value

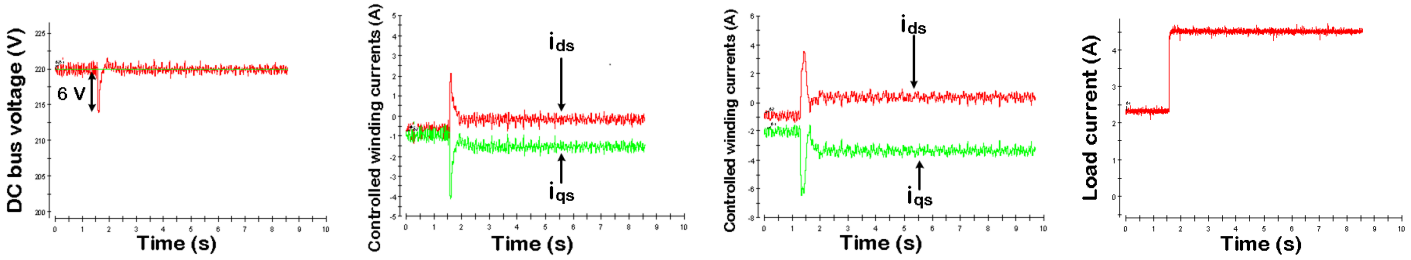

(a) (b) (c) (d)

Fig. 10. (a) DC Bus voltage dynamics due to a step change in load for $k = 0.2$. Response of controlled-winding currents for (b) $k = 0.2$ and (c) $k = 0.4$. (d) Discrete change in load current from 2.27 A to 4.54 A

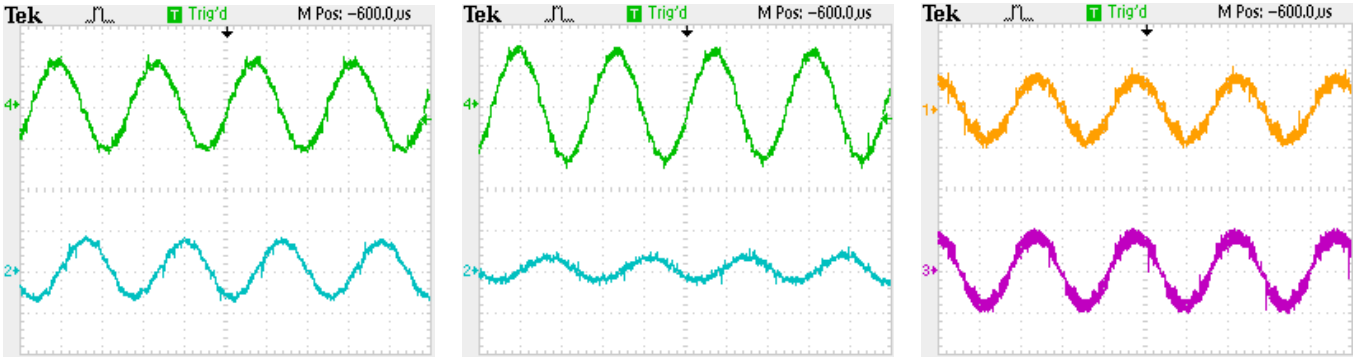

(a) (b) (c)

Fig. 11. Line current waveforms of controlled (CH2, Scale:4 A/div.) and uncontrolled (CH4, Scale: 4 A/div.) winding current at an output power of 1 kW for (a) k=0.4 and (b) k=0.2. (c) Phase voltage waveform (Scale:200 V/div.) of uncontrolled and controlled winding for k=0.2

of i_{ds} is 0.6 A for $k = 0.4$ while it is 0.35 A for $k = 0.2$. This indicates the closeness of simulation and experimental results. Also, i_{qs} changes in proportion to k, as evident from Fig. 10(b) and 10(c).

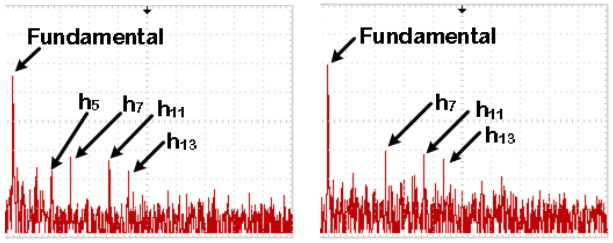

(a) (b)

Fig. 12. Spectra of the line-current of (a) controlled-winding and (b) uncontrolled-winding for $P_{out} = 1$ kW and $k = 0.4$

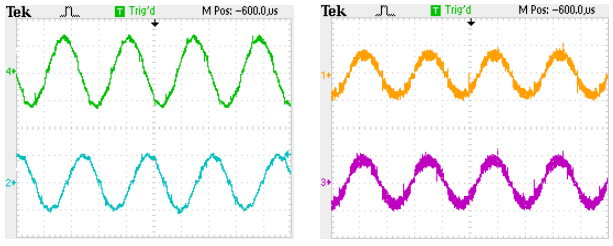

(a) (b)

Fig. 13. (a) Line current waveforms of controlled-winding (CH2, Scale:5A/div) and uncontrolled-winding(CH4, Scale:5A/div) at rated load (b) Phase voltage waveforms (Scale:200 V/div.) at same condition

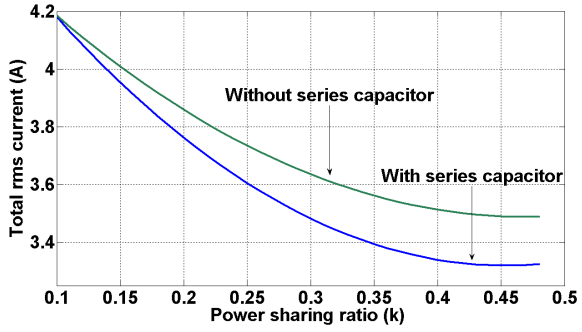

(a)

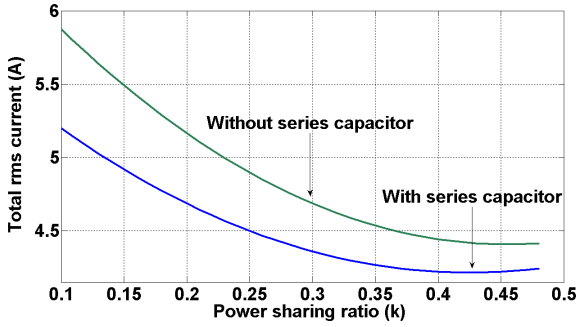

(b)

Fig. 14. Variation of total rms current with power sharing ratio for a load of (a) 1 kW and (b) 1.3 kW

B. Steady-state waveforms and load characteristics

This subsection reports the steady-state performance of the generation system for a fixed speed of 1500 rpm. Fig. 11 shows the line current and phase voltage waveforms. The variation of

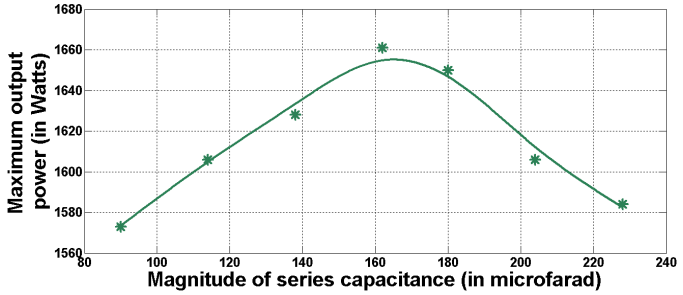

Fig. 15. Variation of maximum output power with the magnitude of per-phase series capacitance corresponding to rated speed of operation

rms values of line current with the variation in k is studied. For a load of 1 kW and $k = 0.4$, I_{UW} is 2.96 A and I_{CW} is 2.26 A. When the value of k is reduced to 0.2, I_{UW} increases to 3.74 A and I_{CW} reduces to 0.8 A, which indicates that current share of each winding can be governed by power sharing factor. Deployment of tuned passive filter assists in improving current quality to a large extent. The fifth and seventh harmonic components in uncontrolled-winding current is reduced to <1% and 3.16% respectively while that of controlled-winding is lowered to 2% and 3.16% respectively, as shown in Fig. 12. The THD of I_{UW} at $k = 0.4$ is 4.89% while that for I_{CW} at same value of k is 5.8 %. Since the rms value of phase voltage does not undergo a significant change with change in value of k, only a waveform corresponding to $k = 0.4$ has been demonstrated. The line-current and phase-voltage waveforms at rated load have been displayed in Fig. 13. The rms value of uncontrolled-winding line current is 4.51 A (with a THD of 4.77%) while that of controlled-winding is 3.5 A (with a THD of 4.92%). The total reactive power demand of the generator system corresponding to the rated load of operation is found to be $Q_{tot} = 1274.38$ VAR. The shunt capacitors and series capacitors are able to provide reactive power support of 389 VAR and 591 VAR respectively. The apparent power handled by the converter in the presence and absence of series capacitors is 691.66 VA and 1083.6 VA respectively. Therefore, the inclusion of series capacitors allow a 36% reduction in apparent power rating of controlled converter.

Performance comparison against configuration with shunt filter only: Fig. 14 shows the variation of total rms current with power sharing ratio for two different loads of 1 kW and 1.3 kW, where total rms current is defined as $I_{tot} = \sqrt{I_{UW}^2 + I_{CW}^2}$. From the plots, it can be seen that I_{tot} is less for the configuration with series capacitor than the configuration with shunt capacitor, corresponding to a particular value of k and load. Series capacitor assists in raising the magnitude of terminal voltage of uncontrolled winding (as evident from the phasor diagram in Fig. 2(c)) and reduces the angle between the terminal voltage and current of uncontrolled winding. Thus, I_{tot} reduces and the overall power-factor within the generation system improves. The power available from the machine can be enhanced. The minimum value of I_{tot} corresponding to 1 kW is 3.23 A with series capacitance and 3.48 A without series capacitance. For a load of 1.3 kW, the minimum value of I_{tot} is 4.2 A and 4.4 A with and without series capacitors respectively.

Fig. 15 demonstrates the variation of maximum output power with the magnitude of series capacitance. The voltage drop across the series capacitance at rated value of uncontrolled winding current is given by $V_{cse} = \frac{I_{ur}}{\omega_e C_{se}}$, where I_{ur} denotes the rms value of uncontrolled-winding current at rated load. With the decrease in the value of C_{se}, the voltage drop across it and the corresponding terminal voltage across uncontrolled-winding increases. Therefore, with the reduction in the value of C_{se}, more active power can be extracted from the generation system. However, further decrease in C_{se} causes even higher terminal voltage across uncontrolled winding which pushes the machine into saturation region. This creates higher reactive power demand and the active power output capability of the machine degrades. This is experimentally validated in the plot shown in Fig. 15. Compared to the configuration with shunt passive filter only, the maximum output power which can be obtained is 1.45 kW. Proper choice of C_{se} will result in enhancing the maximum power output to 1.66 kW. A 14.55% increase in P_{max} is noted which makes the scheme beneficial compared to that reported in [29].

C. Operation at different prime mover speeds

The performance of generating system for different prime-mover speeds has been experimentally investigated (considering wind power generation as the target application) and reported in this sub-section. Since $P_{out} \propto \omega_r^3$ for wind electrical systems, major share of active power takes place through the controlled-winding in the low-speed region where the total output power does not exceed the rating of CWSC. Fig. 16(a) shows the controlled-winding voltages and currents at a speed of 1000 rpm (0.66 p.u.) corresponding to an output power of 0.2963 p.u.. The value of I_{CW} is 3.44 A and the corresponding THD is 2.88%. Similar waveforms have been demonstrated for a speed of 900 rpm (0.6 p.u.) and 0.216 p.u. output power in Fig. 16(b) where the rms value of I_{CW} is 2.95 A with a THD of 2.57%. The steady-state values of i_{ds} and i_{qs} are 1.7 A and -3.7 A respectively, which has close resemblance with the values attained through simulation results shown in Fig. 9(b). The minimum speed required to regulate the output voltage to 220 V is 800 rpm (0.533 p.u.) with an output power of 0.152 p.u. Corresponding result is shown Fig. 16(c). Here, I_{CW} settles at 2.76 A.

VII. Conclusion

A different configuration of DSWIG for a standalone dc generation system has been reported. The major aim is to improve output voltage regulation and power quality within the generating system through a combination of passive tuned filters and series capacitors. While passive tuned filters can absorb the predominant lower order harmonics and supply approximately fixed amount of reactive power, series capacitors will provide reactive power support in proportion to load current. Thus the system attains self-regulating characteristics by selecting proper values of series capacitance. A study shows that stability of the system improves with the increase in load. Compared to shunt-only compensation based system, the proposed configuration offers better power factor and extracts more active power. A simple method to select the magnitude of C_{se} is also discussed. Simulation studies have been conducted on MATLAB/Simulink and corresponding results have been presented. Experimental results obtained using a dSPACE 1103 based laboratory prototype has been provided. Both simulation and experimental results confirm the effectiveness of the proposed configuration in improving voltage regulation in a DSWIG based standalone dc system. Experimental investigations reveal proper choice of series capacitor can enhance the output power by about 15%.

Acknowledgement

The authors acknowledge the support from Department of Science and Technology(DST), Government of India through the

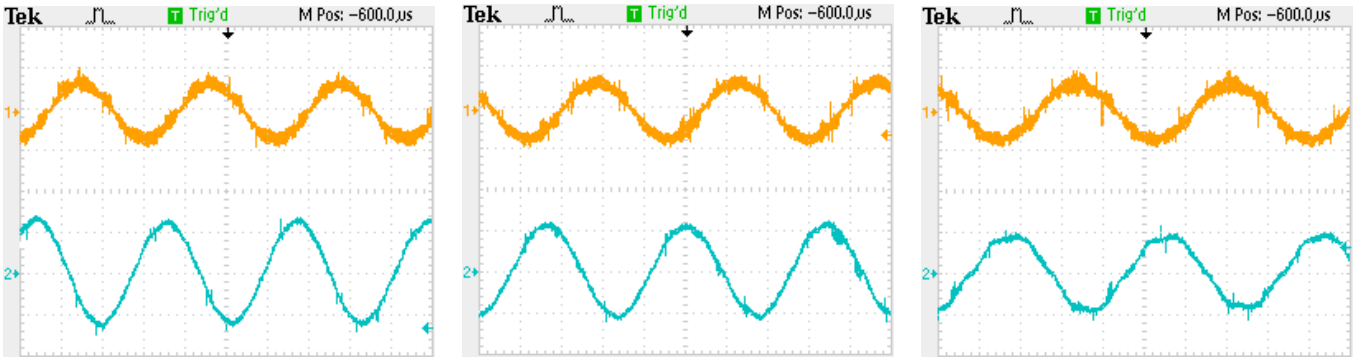

(a) (b) (c)

Fig. 16. Controlled-winding voltage (CH1, Scale: 200 V/div.) and current (CH2, Scale:4 A/div.) for prime-mover speeds of (a)1000 rpm, (b)900 rpm, (c)800 rpm

project "Reliable and Efficient System for Community Energy Solution (RESCUES)" with joint collaboration of DST, India and Engineering and Physical Research Council (EPSRC), UK.

APPENDIX A
MACHINE PARAMETERS

Machine parameters and magnetization curve are presented in Table-I and Fig. 17.

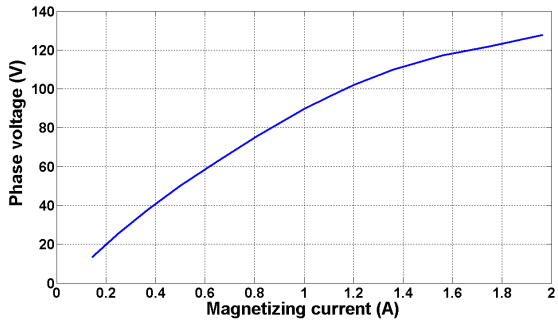

Fig. 17. Magnetization curve of the machine at 50 Hz (as seen from the controlled winding side)

TABLE I. MACHINE RATINGS AND PARAMETERS

Symbol	Parameter	Nominal Value
$I_{s(rated)}$	Rated current of controlled Winding	2.3 A
$I_{u(rated)}$	Rated current of uncontrolled winding	4.5 A
$V_{(rated)}$	Rated voltage of each winding	100 V
P	Number of poles	4
R_s	Resistance of controlled winding	6.33 Ω
R_u	Resistance of uncontrolled winding	5.64 Ω
R_r	Resistance of rotor bars	2.96 Ω
L_m	Magnetizing inductance (unsaturated value)	300.48 mH
L_{us}	Mutual inductance between controlled and uncontrolled winding (unsaturated value)	296.24 mH
L_{ls}	Controlled winding leakage inductance	9.23 mH
L_{lu}	Uncontrolled winding leakage inductance	6.56 mH
L_{lr}	Rotor leakage inductance	7.89 mH
L_f	Shunt filter inductance at uncontrolled winding side	12 mH, 1 A
C_f	Shunt filter capacitance at uncontrolled winding side	48 μF, 100 V
C_{dc}	DC-link capacitor	2200 μF, 315 V

APPENDIX B
WINDING CONFIGURATIONS OF STATOR WINDINGS

The generic configuration of a DSWIG-DC system is demonstrated in Fig. 18. This section illustrates the limitations which arises if both the stator windings are connected in star with unity turns ratio between them. Let, V_{cdc} be the dc bus voltage on the controlled winding side converter. The maximum rms value which CWSC can impress on CW is given by $V_{CW} = \frac{V_{cdc}}{\sqrt{2}}$. For unity turns ratio, $V_{CW} = V_{UW}$. In such a situation, the maximum

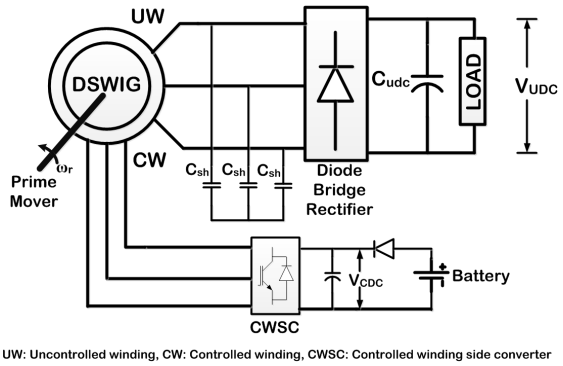

Fig. 18. Generic configuration of dual stator winding induction generator with two isolated dc buses.

output voltage of the diode bridge rectifier on the UW side (at no-load) is given by:

$$V_{udc} = \frac{3\sqrt{2}}{\pi} V_{UW} = \frac{3}{\pi} V_{cdc} \tag{B1}$$

Under loaded condition, the output voltage V_{ucdc} will reduce even further. From (B1), it is evident that it is a buck-type operation from CW side to UW side. Therefore, the output of the diode-bridge rectifier and the PWM-controlled converter cannot be connected in parallel. Connecting the CW in delta and UW in star, a voltage gain of $\sqrt{3}$ is introduced and the two dc buses can be merged into a single one.

REFERENCES

[1] Y. Yao, A. Cosic, and C. Sadarangani, "Power Factor Improvement and Dynamic Performance of an Induction Machine With a Novel Concept of a Converter-Fed Rotor," *IEEE Trans. Energy Convers.*, vol. 31, no. 2, pp. 769–775, June 2016.

[2] N. K. S. Naidu and B. Singh, "Doubly Fed Induction Generator for Wind Energy Conversion Systems With Integrated Active Filter Capabilities," *IEEE Trans. Ind. Informat.*, vol. 11, no. 4, pp. 923–933, Aug 2015.

[3] Y. Song and H. Nian, "Enhanced Grid-Connected Operation of DFIG Using Improved Repetitive Control Under Generalized Harmonic Power Grid," *IEEE Trans. Energy Convers.*, vol. 30, no. 3, pp. 1019–1029, Sept 2015.

[4] S. Mondal and D. Kastha, "Improved Direct Torque and Reactive Power Control of a Matrix-Converter-Fed Grid-Connected Doubly Fed Induction Generator," *IEEE Trans. Ind. Electron.*, vol. 62, no. 12, pp. 7590–7598, Dec 2015.

[5] F. Blaabjerg and K. Ma, "Future on Power Electronics for Wind Turbine Systems," *IEEE J. Emerg. Sel. Topics Power Electron.*, vol. 1, no. 3, pp. 139–152, Sept 2013.

[6] F. Barati, R. McMahon, S. Shao, E. Abdi, and H. Oraee, "Generalized Vector Control for Brushless Doubly Fed Machines With Nested-Loop Rotor," *IEEE Trans. Ind. Electron.*, vol. 60, no. 6, pp. 2477–2485, June 2013.

[7] J. Chen, W. Zhang, B. Chen, and Y. Ma, "Improved Vector Control of Brushless Doubly Fed Induction Generator under Unbalanced Grid Conditions for Offshore Wind Power Generation," *IEEE Trans. Energy Convers.*, vol. 31, no. 1, pp. 293–302, March 2016.

[8] B. Singh, S. S. Murthy, and R. S. R. Chilipi, "STATCOM-Based Controller for a Three-Phase SEIG Feeding Single-Phase Loads," *IEEE Trans. Energy Convers.*, vol. 29, no. 2, pp. 320–331, June 2014.

[9] M. Bai and D. Vukadinovi, "Online Efficiency Optimization of a Vector Controlled Self-Excited Induction Generator," *IEEE Trans. Energy Convers.*, vol. 31, no. 1, pp. 373–380, March 2016.

[10] S. Basak and C. Chakraborty, "Dual Stator Winding Induction Machine: Problems, Progress, and Future Scope," *IEEE Trans. Ind. Electron.*, vol. 62, no. 7, pp. 4641–4652, July 2015.

[11] A. R. Munoz and T. A. Lipo, "Dual stator winding induction machine drive," *IEEE Trans. Appl. Ind.*, vol. 36, no. 5, pp. 1369–1379, Sep 2000.

[12] J. M. Guerrero and O. Ojo, "Total Airgap Flux Minimization in Dual Stator Winding Induction Machines," *IEEE Trans. Power Electron.*, vol. 24, no. 3, pp. 787–795, March 2009.

[13] N. A. Azeez, K. Gopakumar, J. Mathew, and C. Cecati, "A Harmonic Suppression Scheme for Open-End Winding Split-Phase IM Drive Using Capacitive Filters for the Full Speed Range," *IEEE Trans. Ind. Electron.*, vol. 61, no. 10, pp. 5213–5221, Oct 2014.

[14] K. Hatua and V. T. Ranganathan, "A Novel VSI- and CSI-Fed Active Reactive Induction Motor Drive with Sinusoidal Voltages and Currents," *IEEE Trans. Power Electron.*, vol. 26, no. 12, pp. 3936–3947, Dec 2011.

[15] O. Ojo and I. Davidson, "PWM-VSI Inverter-Assisted Stand-Alone Dual Stator Winding Induction Generator," *IEEE Trans. Appl. Ind.*, vol. 36, no. 6, pp. 1604–1611, Nov 2000.

[16] M. Naidu and J. Walters, "A 4-kW 42-V Induction-Machine-Based Automotive Power Generation System With a Diode Bridge Rectifier and a PWM Inverter," *IEEE Trans. Appl. Ind.*, vol. 39, no. 5, pp. 1287–1293, Sept 2003.

[17] F. Bu, Y. Hu, W. Huang, and S. Zhuang, "Parameter Design and Static Performance of Dual Stator-Winding Induction Generator Variable Frequency AC Generating System With Inductive and Capacitive Loads," *IEEE Trans. Ind. Electron.*, vol. 61, no. 8, pp. 3902–3914, Aug 2014.

[18] Y. Li, Y. Hu, W. Huang, L. Liu, and Y. Zhang, "The Capacity Optimization for the Static Excitation Controller of the Dual-Stator-Winding Induction Generator Operating in a Wide Speed Range," *IEEE Trans. Ind. Electron.*, vol. 56, no. 2, pp. 530–541, Feb 2009.

[19] F. Bu, W. Huang, Y. Hu, and K. Shi, "An Excitation-Capacitor-Optimized Dual Stator-Winding Induction Generator With the Static Excitation Controller for Wind Power Application," *IEEE Trans. Energy Convers.*, vol. 26, no. 1, pp. 122–131, March 2011.

[20] F. Bu, Y. Hu, W. Huang, and S. Zhuang, "Parameter Design and Static Performance of Dual Stator-Winding Induction Generator Variable Frequency AC Generating System With Inductive and Capacitive Loads," *IEEE Trans. Ind. Electron.*, vol. 61, no. 8, pp. 3902–3914, Aug 2014.

[21] M. Moradian and J. Soltani, "An Isolated Three-Phase Induction Generator System With Dual Stator Winding Sets Under Unbalanced Load Condition," *IEEE Trans. Energy Convers.*, vol. 31, no. 2, pp. 531–539, June 2016.

[22] F. Bu, Y. Hu, W. Huang, S. Zhuang, and K. Shi, "Wide-Speed-Range-Operation Dual Stator-Winding Induction Generator DC Generating System for Wind Power Applications," *IEEE Trans. Power Electron.*, vol. 30, no. 2, pp. 561–573, Feb 2015.

[23] H. Xu, F. Bu, W. Huang, Y. Hu, H. Liu, and Y. Zhao, "Analysis, Comparison, and Discussion of Control Strategies for Dual Stator-Winding Induction Generator DC Generating System," *IEEE J. Emerg. Sel. Topics Power Electron.*, vol. 4, no. 3, pp. 1007–1014, Sept 2016.

[24] Z. Wu, O. Ojo, and J. Sastry, "High-Performance Control of a Dual Stator Winding DC Power Induction Generator," *IEEE Trans. Appl. Ind.*, vol. 43, no. 2, pp. 582–592, March 2007.

[25] M. F. Iacchetti, G. D. Marques, and R. Perini, "Torque Ripple Reduction in a DFIG-DC System by Resonant Current Controllers," *IEEE Trans. Power Electron.*, vol. 30, no. 8, pp. 4244–4254, Aug. 2015.

[26] G. D. Marques and M. F. Iacchetti, "Minimization of Torque Ripple in the DFIG-DC System via Predictive Delay Compensation," *IEEE Trans. Ind. Electron. (in early access)*.

[27] G. D. Marques, D. M. Sousa, and M. F. Iacchetti, "Air-Gap Power-Based Sensorless Control in a DFIG Connected to a DC Link," *IEEE Trans. Energy Convers.*, vol. 30, no. 1, pp. 367–375, Mar. 2015.

[28] H. Misra, A. Gundavarapu, and A. K. Jain, "Control Scheme for DC Voltage Regulation of Stand-Alone DFIG-DC System," *IEEE Trans. Ind. Electron.*, vol. 64, no. 4, pp. 2700–2708, Apr. 2017.

[29] S. Basak and C. Chakraborty, "A New Optimal Current Control Technique for Dual Stator Winding Induction Generator," *IEEE J. Emerg. Sel. Topics Power Electron.*, vol. 5, no. 2, pp. 820–832, Jun. 2017.

[30] N. Mohan, T. M. Undeland, and W. P. Robbins, *Power Electronics. Converters, Applications and Design*, 3rd ed. John Wiley and Sons, Inc, 2003.

[31] C. Chakraborty, S. N. Bhadra, A. K. Chattopadhyay, and S. K. Biswas, "A Novel Two Phase Self Excited Induction Generator-Series Connected Converter System as DC Power Supply," in *Conference Record of the 1994 IEEE Industry Applications Society Annual Meeting, 1994.*, Oct 1994, pp. 38–43 vol.1.

Saptarshi Basak (S'14) received his B.E. degree in Electrical Engineering from Jadavpur University and M. Tech Degree in Electrical Engineering with specialization in Machine, Drives and Power Electronics from Indian Institute of Technology Kharagpur in the year 2010 and 2012 respectively. He is pursuing his Ph.D in the Department of Electrical Engineering, Indian Institute of Technology Kharagpur. His research interests include Design and Control of Brushless Generation Systems, and Estimation Techniques and Control of AC Drives.

Chandan Chakraborty (S'92-M'97-SM'01-F'15) received B.E and M.E degrees in Electrical Engineering from Jadavpur University in 1987 and 1989 respectively and Ph.D degrees from Indian Institute of Technology Kharagpur and Mie University, Japan in 1997 and 2000 respectively. Presently, he is a professor in the Department of Electrical Engineering, Indian Institute of Technology Kharagpur. His research interest includes power converters, motor drives, electric vehicles and renewable energy.

Dr. Chakraborty was awarded the JSPS Fellowship to work at the University of Tokyo during 2000-2002. He has received the Bimal Bose award in power electronics in 2006 from the IETE (India). He has regularly contributed to IES conferences such as IECON, ISIE and ICIT as technical program chair/track chair. He is an ADCOM member of the IEEE Industrial Electronics Society. He is one of the Associate Editors of IEEE Transactions on Industrial Electronics and IEEE Industrial Electronics Magazine and an Editor of the IEEE Transactions on Sustainable Energy. He is the Founding Editor-in-Chief of IE Technology News (ITeN), a web-only publication for IEEE Industrial Electronics Society. He is a Fellow of IEEE and Indian National Academy of Engineering (INAE).

Bikash C. Pal (M'00-SM'02-F'13) is Professor of Power Systems at Imperial College London. He is research active in power system stability, control and computation. Prof. Pal has graduated 17 PhDs and published 70 technical papers in IEEE Transactions and IET journals. He has co-authored two books and two award winning IEEE Task Force/Working Group reports. He is Editor-in-Chief of IEEE Transactions on Sustainable Energy and Fellow of IEEE for his contribution to power system stability and control.